Computers, Materials & Continua

Tech Science Press

https://doi.org/10.32604/cmc.2026.086653

ARTICLE

# A Physics-Guided Machine Learning Framework Linking Carbon Concentration, Phase Constitution, and Wear Behavior in Carburized SCR420 Steel

**Gi-Hoon Kwon, Byoungho Choi, Kyong Jun An, Hyosoo Jeon and Kyoung Il Moon***

Customized Manufacturing R&D Department (Siheung Technology Support Center), Korea Institute of Industrial Technology, Siheung, Republic of Korea

*Corresponding Author: Kyoung Il Moon. Email: klmoon@kitech.re.kr

Received: 03 June 2026; Accepted: 25 August 2026; Published: 22 October 2026

**ABSTRACT:** A physics-guided machine-learning framework was developed to investigate the relationships among carbon concentration, phase constitution, hardness, and wear behavior in carburized SCR420 steel. Surface carbon concentrations of 0.5–0.9 wt.%C were produced by vacuum carburizing, followed by hardness, XRD, friction, and wear measurements. Experimentally measured descriptors were integrated with physics-based descriptors derived from JMatPro thermodynamic and phase-transformation simulations to predict wear behavior. JMatPro successfully reproduced the overall experimental trends in hardness and phase evolution, showing good agreement with the experimental measurements. Among the investigated models, CatBoost achieved the highest predictive performance ($R^2$ = 0.990, RMSE = 1.163 × $10^{-6}$ $mm^3$/N·m). SHAP analysis identified friction coefficient, hardness, and phase constitution as the most important contributors to the CatBoost model output. An optimal surface carbon concentration range of 0.79–0.85 wt.%C was identified for improved wear resistance. The proposed framework demonstrates the potential of integrating physics-based simulations with explainable machine learning for data-driven optimization of carburizing processes.

**KEYWORDS:** Carburizing; carbon concentration; wear behavior; physics-guided machine learning; explainable artificial intelligence (XAI); process optimization

## 1 Introduction

Carburizing is one of the most widely used thermochemical surface-hardening processes for mechanical components subjected to high contact stresses and cyclic loading, such as gears, shafts, bearings, and power-transmission parts [1,2]. By combining carburizing with subsequent quenching, a hardened surface layer with excellent wear resistance and fatigue strength can be achieved while maintaining a tough core region [2,3]. Owing to these advantages, low-alloy carburizing steels such as SCR420 are extensively used in automotive and industrial machinery applications.

The performance of carburized steels is strongly dependent on the final surface carbon concentration. Surface carbon concentration governs phase transformation behavior during quenching, thereby influencing the fractions of martensite and retained austenite as well as the resulting hardness distribution [3,4]. In general, increasing carbon concentration enhances hardness and wear resistance; however, excessive carbon enrichment may promote retained austenite formation, leading to reduced dimensional stability and degraded tribological performance [2,5]. Therefore, a quantitative understanding of the relationships

Copyright © 2026 The Authors. Published by Tech Science Press. This work is licensed under a Creative Commons Attribution 4.0 International License, which permits unrestricted use, distribution, and reproduction in any medium, provided the original work is properly cited.

among carbon concentration, phase constitution, hardness, and wear behavior is essential for optimizing carburizing processes.

Retained austenite plays a particularly important role in determining the mechanical and tribological properties of carburized steels. Previous studies have reported that retained austenite can improve wear resistance through the transformation-induced plasticity (TRIP) effect [6]. However, excessive retained austenite may also induce localized deformation and surface delamination under repeated contact loading, thereby reducing wear resistance [4,5]. Consequently, the wear behavior of carburized steels cannot be explained solely by hardness and should be interpreted in conjunction with phase constitution and microstructural evolution.

In recent years, computational materials engineering tools such as JMatPro have been widely employed to predict phase transformation behavior during carburizing and quenching processes [7–9]. Based on alloy composition and heat-treatment conditions, JMatPro can estimate phase fractions and hardness with reasonable accuracy and has been successfully applied to various steel systems. Nevertheless, studies linking simulation-derived physical descriptors to experimentally measured wear behavior remain limited.

At the same time, machine learning (ML) has emerged as a powerful tool for materials-property prediction and process optimization in materials science and engineering [10–12]. Recent studies have increasingly explored the integration of physics-based simulations with machine learning to improve prediction accuracy and model interpretability in materials design [13–17]. In particular, simulation-derived descriptors obtained from thermodynamic and phase-transformation calculations can provide physically meaningful information that complements experimental measurements. However, few studies have systematically integrated experimentally measured descriptors with simulation-derived physical descriptors to investigate the relationships among carbon concentration, phase constitution, hardness, friction coefficient, and wear behavior in carburized steels.

Therefore, in the present study, the effects of surface carbon concentration on phase constitution, hardness, friction behavior, and wear performance of carburized SCR420 steel were systematically investigated. A physics-guided machine-learning framework was developed by integrating experimentally measured descriptors with physics-based descriptors derived from JMatPro thermodynamic and phase-transformation simulations, including hardness and phase fractions. These simulation-derived descriptors were incorporated as complementary physical information to improve wear-rate prediction and model interpretation. Pearson correlation analysis, feature-importance evaluation, and SHAP-based explainable artificial intelligence were employed to interpret the model outputs. Finally, an AI-guided design window for enhanced wear resistance was established, providing a practical strategy for data-driven optimization of carburizing processes. Unlike physics-informed learning frameworks that explicitly embed governing equations into the optimization process, the present framework incorporates physics-based simulation results as complementary descriptors to improve predictive performance and model interpretability.

## 2 Experimental Procedure

### *2.1 Material and Carburizing Treatment*

Commercial low-alloy carburizing steel SCR420 was used in this study. Cylindrical specimens with a diameter of 30 mm and a height of 10 mm were prepared. The chemical composition of the SCR420 steel was 0.21C–0.72Mn–1.05Cr–0.24Ni–0.23Si (wt.%) with Fe as the balance.

Vacuum carburizing was performed to investigate the effects of surface carbon concentration on phase constitution and wear behavior. The carburizing treatment was carried out using a quartz horizontal tube furnace (hot zone: 100 mm in diameter and 260 mm in length). Carburizing was conducted at 950°C using acetylene ($C_2H_2$) as the carbon source. The gas flow rate and process pressure were maintained at 30 sccm and

10 Torr, respectively. Seventeen target surface carbon concentrations ranging from 0.50 to 0.90 wt.%C were achieved by adjusting the boost and diffusion times. The carburizing schedules were designed to establish the target carbon concentration within approximately 0.1 mm from the surface, which is directly associated with wear behavior.

After carburizing, all specimens were oil-quenched without tempering. Five repeated experiments were performed for each condition, resulting in a total dataset of 85 samples. Representative carburizing conditions for surface carbon concentrations of 0.5, 0.6, 0.7, 0.8, and 0.9 wt.%C are listed in Table 1.

**Table 1:** Representative vacuum carburizing schedules used to achieve target surface carbon concentrations in SCR420 steel.

| Target Surface Carbon Content (wt.%C) | Carburizing Temperature (°C) | Total Boost Time (s) | Total Diffusion Time (s) | $C_2H_2$ Flow Rate (sccm) | Pressure (Torr) |
|---|---|---|---|---|---|
| 0.5 | 950 | 240 | 4360 | 30 | 10 |
| 0.6 | | 420 | 3960 | | |
| 0.7 | | 840 | 3060 | | |
| 0.8 | | 1050 | 2360 | | |
| 0.9 | | 1400 | 1660 | | |

### *2.2 Microstructural and Tribological Characterization*

Carbon concentration profiles were measured using an electron probe microanalyzer (JXA-8500F, JEOL, Japan). Hardness distributions were evaluated using a micro-Vickers hardness tester (HM-210B, Mitutoyo, Japan) under a load of 100 g (Hv0.1). For each condition, five measurements were performed and the average value was used for subsequent analysis.

Phase constitution was analyzed by X-ray diffraction (D8 Focus, Bruker, Germany) using Cu-Kα radiation over a 2θ range of 40°–100° with a step size of 0.02° and a scan rate of 2°/min. Prior to phase quantification, the diffraction profiles were baseline-corrected to minimize background contributions, and the diffraction peaks corresponding to martensite (α′) and retained austenite (γ) were identified. The phase fractions were then determined from the relative integrated intensities of the corresponding diffraction peaks using the integrated-intensity method.

Tribological properties were evaluated using a ball-on-disk tribometer (JLTB-02, J&L Tech, Republic of Korea). A 6-mm-diameter SUJ2 steel ball was used as the counterface material. Wear tests were conducted under a normal load of 10 N, a sliding speed of 0.1 m/s, and a total sliding distance of 500 m. The friction coefficient was continuously recorded during testing, and the wear rate was calculated from the wear-track geometry. In addition, the wear mechanisms were investigated by scanning electron microscopy (NNS-450, FEI, USA) observations of the wear tracks after testing.

### *2.3 JMatPro Simulation*

To predict the phase constitution and hardness as a function of surface carbon concentration, thermodynamic and phase-transformation simulations were performed using the Steel Module of JMatPro (Sente Software Ltd., UK). The chemical composition of SCR420 steel (0.21C–0.72Mn–1.05Cr–0.24Ni–0.23Si, wt.%, Fe balance) and the experimentally measured surface carbon concentrations were used as input parameters to calculate the martensite fraction, retained austenite fraction, and hardness.

The calculated results were validated through comparison with the experimental hardness and XRD measurements. The predictive performance was quantitatively evaluated using the coefficient of

determination ($R^2$), mean absolute error (MAE), root mean square error (RMSE), and mean bias. Subsequently, the predicted hardness and phase fractions were incorporated into the machine-learning model as physics-based descriptors derived from thermodynamic and phase-transformation simulations. These descriptors were integrated with the experimentally measured variables to provide complementary physical information for wear-rate prediction and model interpretation.

### *2.4 Physics-Guided Machine Learning and XAI Analysis*

To establish the physics-guided machine-learning framework, experimentally measured carbon concentration, martensite fraction, retained austenite fraction, hardness, surface roughness, and friction coefficient were used as input variables, while wear rate was selected as the target variable. JMatPro-predicted hardness and phase fractions, derived from thermodynamic and phase-transformation simulations, were incorporated as complementary physics-based descriptors.

Four machine-learning algorithms, including Linear Regression (LR), Random Forest (RF), XGBoost, and CatBoost, were trained using a dataset of 85 samples. An ablation study was conducted using three feature sets: experimental descriptors only, JMatPro-derived descriptors only, and the combined descriptor set. Model performance was first evaluated using conventional random 10-fold cross-validation. To further assess the robustness of the proposed framework and to exclude possible overestimation arising from repeated measurements under the same nominal carburizing condition, additional grouped cross-validation and leave-one-condition-out (LOCO) validation were performed by assigning all five repeated samples from the same target surface carbon concentration to the same validation group. A fixed random seed (42) was used for all cross-validation procedures to ensure reproducibility. The coefficient of determination ($R^2$) and root mean square error (RMSE) were used to evaluate model performance.

Pearson correlation, feature importance, and SHAP (SHapley Additive exPlanations) analyses were performed to interpret the model outputs. The optimized model was subsequently used to establish an AI-guided design window for enhanced wear resistance. A schematic illustration of the proposed physics-guided machine-learning and explainable artificial intelligence (XAI) framework is presented in Fig. 1.

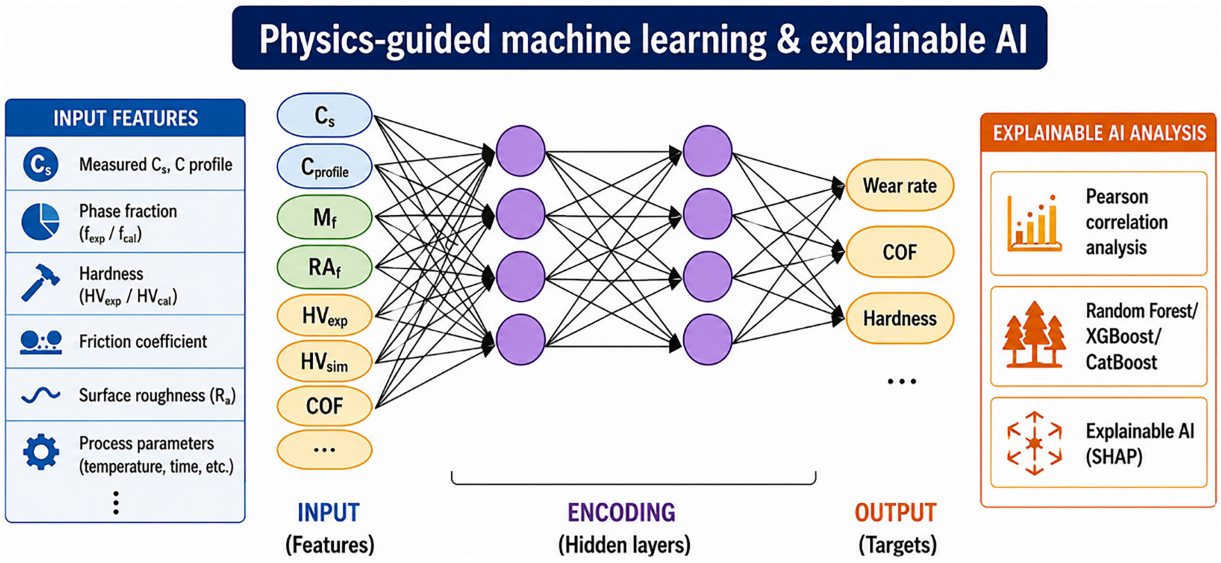



**Figure 1:** Schematic illustration of the physics-guided machine learning and explainable AI framework for predicting wear behavior in carburized SCR420 steel.

## 3 Results and Discussion

### *3.1 Effect of Surface Carbon Concentration on Microstructure and Tribological Behavior*

Fig. 2 presents the carbon concentration profiles of carburized SCR420 steel with different surface carbon concentrations. All specimens exhibited a typical diffusion-controlled carbon gradient, where the carbon concentration was highest at the surface and gradually decreased toward the core region. As the target surface carbon concentration increased, the measured surface carbon content increased from approximately 0.5 to 0.9 wt.%C. Regardless of carburizing condition, the carbon concentration progressively approached the nominal carbon content of the SCR420 substrate (~0.2 wt.%C) at depths of approximately 1.2–1.5 mm. Furthermore, higher surface carbon concentrations resulted in a deeper carbon-enriched layer, indicating that both the surface carbon level and effective case depth were successfully controlled through adjustment of the boost and diffusion stages during vacuum carburizing.

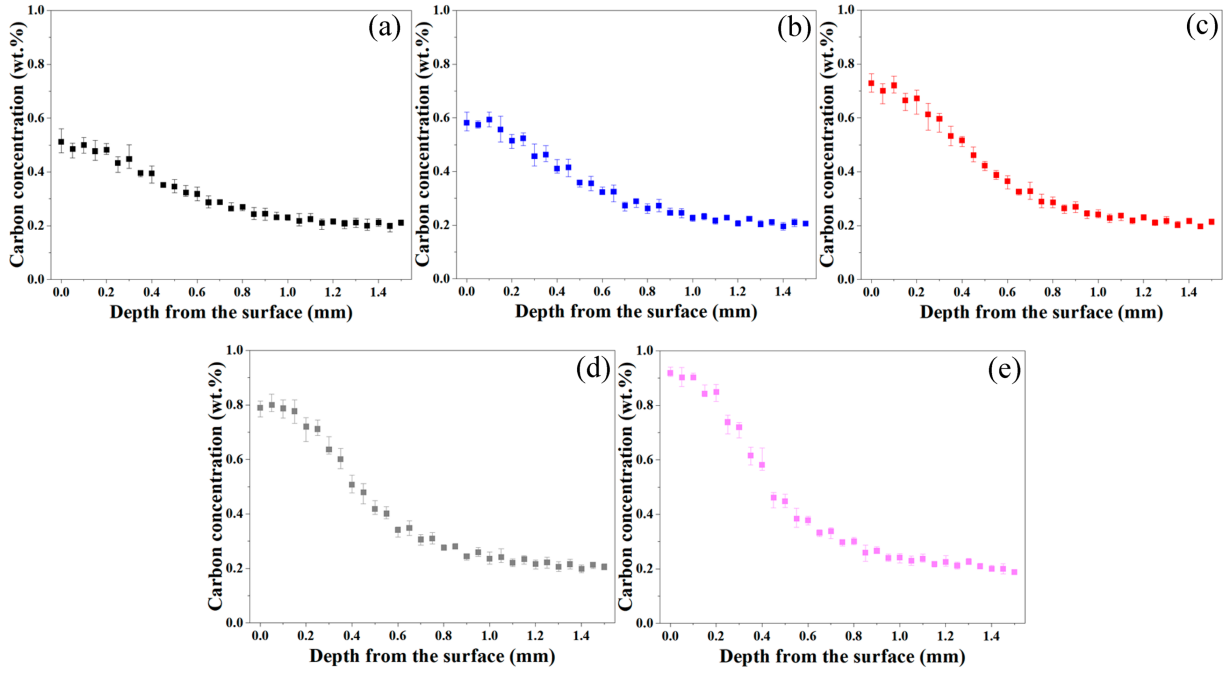



**Figure 2:** Carbon concentration profiles according to surface carbon concentrations: (**a**) 0.5 wt.%C; (**b**) 0.6 wt.%C; (**c**) 0.7 wt.%C; (**d**) 0.8 wt.%C; and (**e**) 0.9 wt.%C.

The corresponding MicroVickers hardness profiles are shown in Fig. 3. All specimens exhibited a typical carburized hardness distribution, characterized by high surface hardness and a gradual decrease toward the core region. The surface hardness increased with increasing surface carbon concentration and exceeded 850 Hv under the highest carbon condition. In addition, the effective hardened depth increased with increasing surface carbon concentration, consistent with the carbon concentration profiles shown in Fig. 2. A clear correlation was observed between carbon concentration and hardness. Regions with higher carbon concentrations exhibited higher hardness values, which can be attributed to the enhanced hardenability and lattice distortion induced by carbon dissolved in the martensitic matrix during quenching. These results indicate that the hardness distribution of carburized SCR420 steel is primarily associated with the carbon concentration profile established during carburizing. Since hardness is closely associated with wear resistance, the observed variations are expected to significantly influence the subsequent tribological behavior.

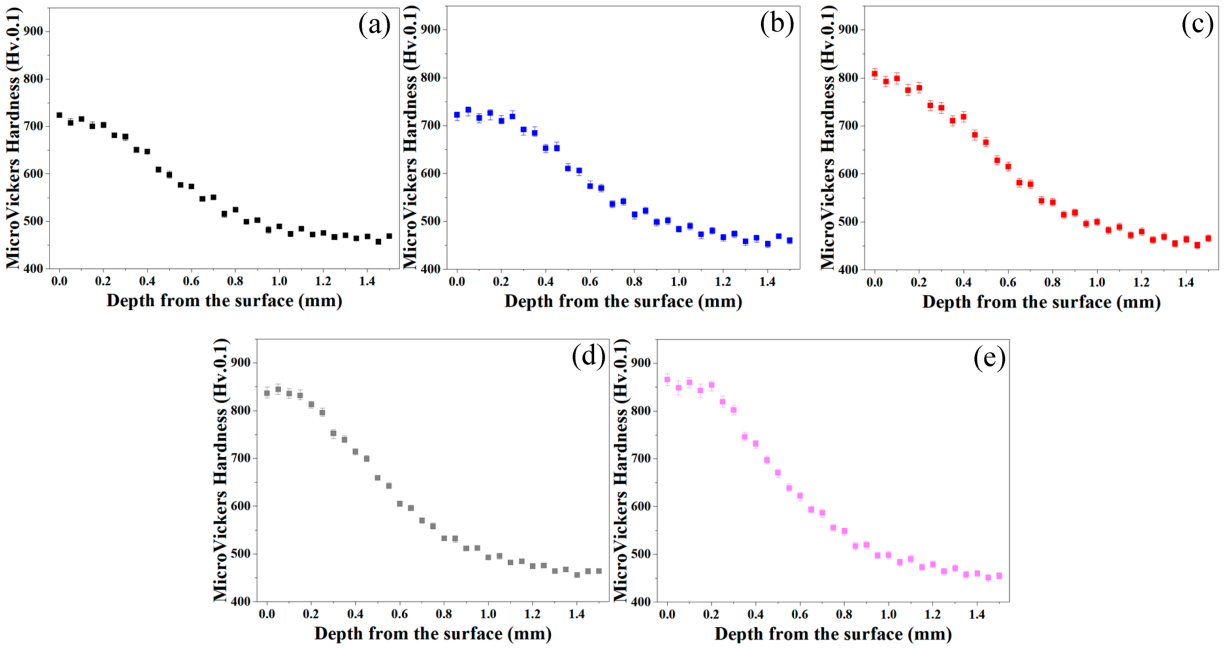



**Figure 3:** MicroVickers Hardness profiles according to surface carbon concentrations: (**a**) 0.5 wt.%C; (**b**) 0.6 wt.%C; (**c**) 0.7 wt.%C; (**d**) 0.8 wt.%C; and (**e**) 0.9 wt.%C.

Fig. 4 shows the surface microstructures of carburized SCR420 steel as a function of surface carbon concentration. All specimens exhibited a predominantly martensitic microstructure after carburizing and oil quenching. However, noticeable microstructural changes were observed with increasing surface carbon concentration. At relatively low carbon concentrations, the microstructure was mainly composed of fine lath martensite with a relatively uniform morphology. As the surface carbon concentration increased, the martensitic structure became denser and more refined, indicating enhanced hardenability during quenching. In addition, localized regions with a darker contrast were observed at higher carbon concentrations, suggesting the presence of retained austenite formed by the stabilization effect of carbon.

The observed microstructural evolution is consistent with the hardness profiles presented in Fig. 3. The refinement of the martensitic structure and the increased carbon supersaturation within the martensite are considered responsible for the progressive increase in surface hardness with increasing carbon concentration. However, excessive carbon enrichment may also promote the formation of retained austenite, which can influence the mechanical and tribological behavior of carburized steels.

Fig. 5 presents the XRD patterns of carburized SCR420 steel with different surface carbon concentrations. All specimens exhibited characteristic diffraction peaks corresponding to martensite ($\alpha'$) and retained austenite ($\gamma$), indicating that the carburized layers consisted predominantly of martensitic microstructures with varying amounts of retained austenite after oil quenching. As the surface carbon concentration increased, the retained austenite peaks became more pronounced, suggesting an increase in the retained austenite fraction. This behavior is attributed to carbon enrichment, which stabilizes austenite and suppresses martensitic transformation during quenching. The increase in retained austenite is consistent with the microstructural observations shown in Fig. 4.

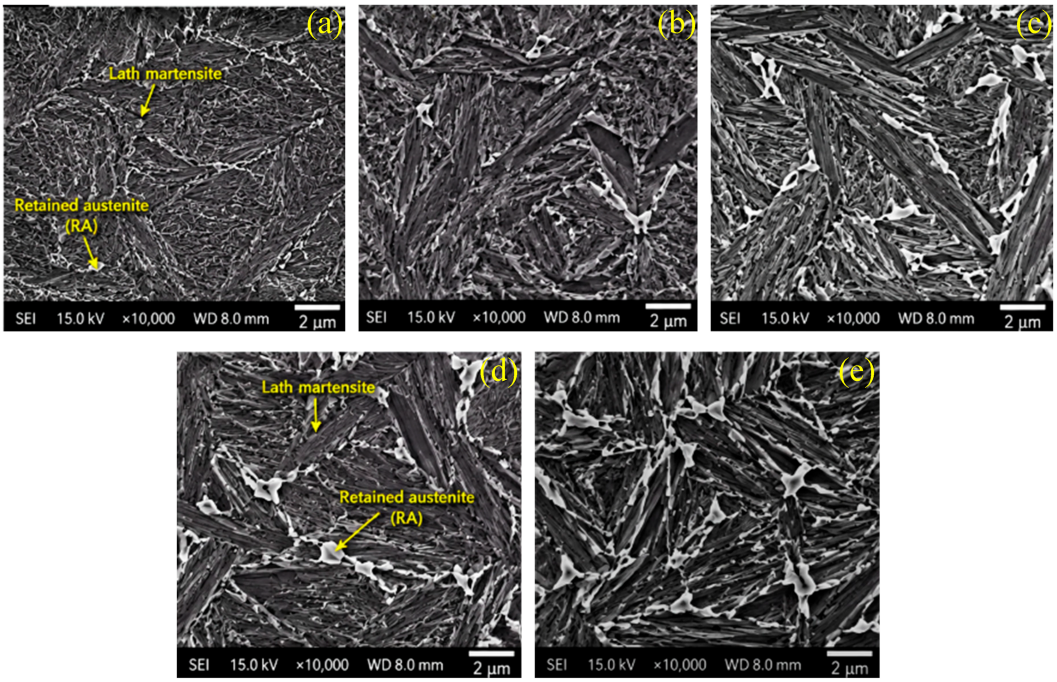



**Figure 4:** Surface microstructural evolution as a function of surface carbon concentrations: (**a**) 0.5 wt.%C; (**b**) 0.6 wt.%C; (**c**) 0.7 wt.%C; (**d**) 0.8 wt.%C; and (**e**) 0.9 wt.%C.

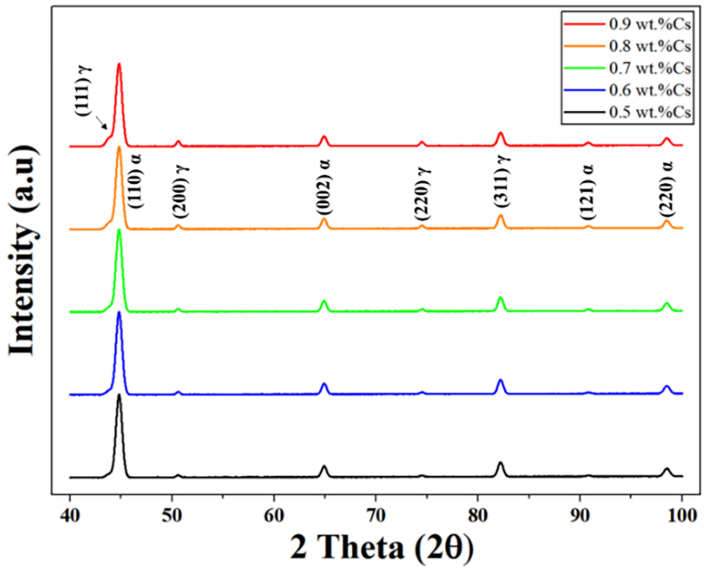



**Figure 5:** XRD patterns of carburized SCR420 steel with different surface carbon contents.

Carbon enrichment not only enhances martensite hardness through solid-solution strengthening but also increases austenite stability [18]. Consequently, the final phase constitution is determined by the balance between martensite formation and retained austenite stabilization. Since both phases strongly influence

hardness and wear behavior, the tribological performance of carburized SCR420 steel should be interpreted in terms of their combined effects rather than carbon concentration alone.

Fig. 6 shows the AFM surface morphologies and average surface roughness ($R_a$) values of carburized SCR420 steel with different surface carbon concentrations. All specimens exhibited relatively similar surface topographies without significant differences in surface morphology. The measured $R_a$ values ranged within a narrow range, indicating that the carburizing conditions had a limited influence on the surface roughness of the specimens.

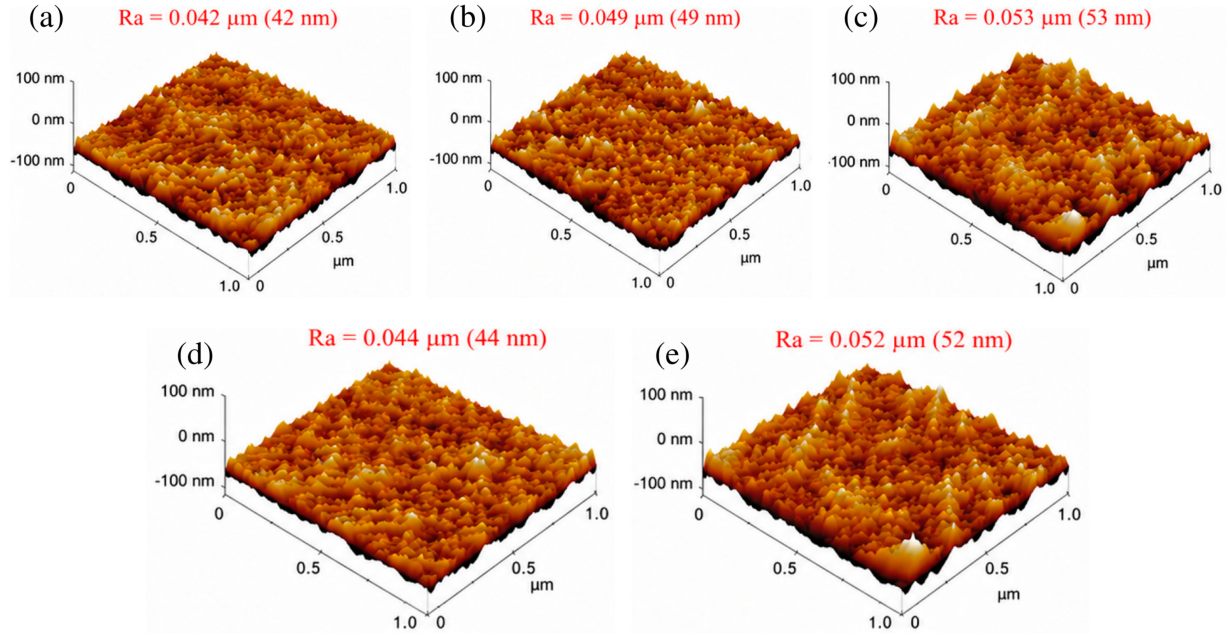



**Figure 6:** AFM surface morphologies and average surface roughness ($R_a$) of carburized SCR420 steel with different surface carbon concentrations: (**a**) 0.5 wt.%C; (**b**) 0.6 wt.%C; (**c**) 0.7 wt.%C; (**d**) 0.8 wt.%C; and (**e**) 0.9 wt.%C.

Although slight variations in roughness were observed depending on the surface carbon concentration, no clear trend was identified. Compared with the substantial changes observed in carbon concentration, hardness, and phase constitution, the variation in surface roughness was relatively minor. Therefore, the differences in tribological behavior observed in this study are unlikely to originate primarily from surface roughness. These results suggest that the friction and wear characteristics of carburized SCR420 steel are more strongly influenced by changes in microstructure, phase constitution, and hardness than by surface roughness. Accordingly, the subsequent tribological behavior is discussed in relation to the combined effects of carbon concentration, martensite fraction, retained austenite fraction, and hardness.

Fig. 7 presents the friction coefficient curves and wear rates of carburized SCR420 steel as a function of surface carbon concentration. As shown in Fig. 7a, all specimens exhibited stable friction behavior after a short running-in period. The average friction coefficient generally decreased with increasing surface carbon concentration, indicating improved sliding performance of the carburized layer. The wear rates summarized in Fig. 7b also decreased with increasing surface carbon concentration, demonstrating enhanced wear resistance. This improvement is closely related to the increased hardness and the evolution of phase constitution observed in Figs. 3–5. The formation of a harder martensitic layer suppresses plastic deformation and material removal during sliding contact [19].

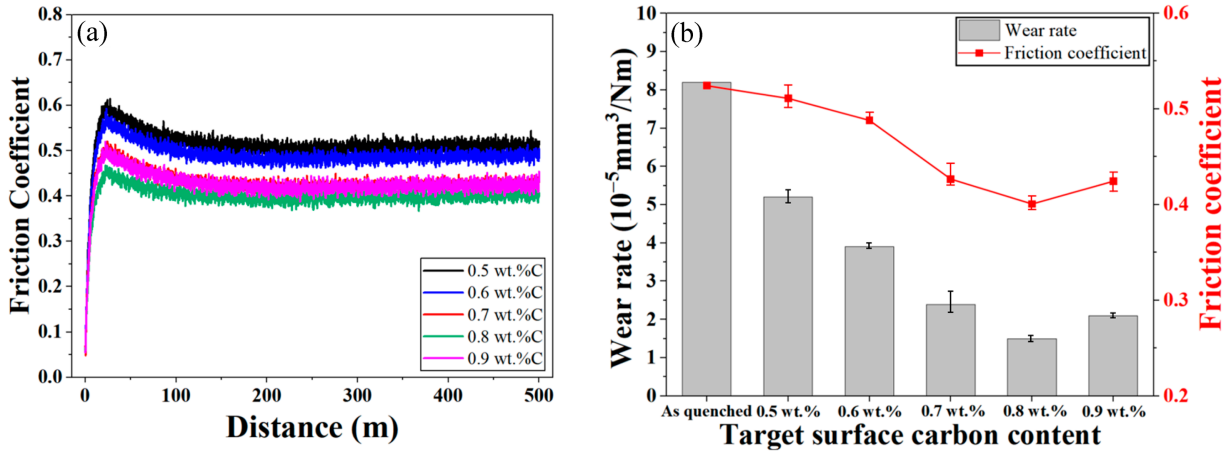



**Figure 7:** Relationship between surface carbon concentration and tribological behavior of carburized SCR420 steel: (**a**) friction coefficient curves measured during ball-on-disk testing and (**b**) average friction coefficient and wear rate as a function of surface carbon concentration.

However, the wear resistance did not improve continuously with increasing carbon concentration. The reduction in wear rate became less pronounced at the highest carbon condition, suggesting that wear behavior is influenced not only by hardness but also by the balance between martensite and retained austenite. Therefore, the tribological performance of carburized SCR420 steel is influenced by the combined effects of carbon concentration, phase constitution, and hardness. These experimental trends suggest the existence of an optimal carbon concentration range, which was subsequently quantified using the trained machine-learning model.

Fig. 8 shows the SEM morphologies of the wear tracks formed on carburized SCR420 steel after ball-on-disk testing. Distinct differences in wear-track characteristics were observed depending on the surface carbon concentration.

At relatively low carbon concentrations, wider wear tracks, pronounced ploughing grooves, and wear debris were observed, indicating severe material removal during sliding contact. In contrast, specimens with higher surface carbon concentrations exhibited narrower and smoother wear tracks with reduced surface damage. The improved wear resistance can be attributed to the formation of a harder carburized layer, which effectively suppressed plastic deformation and abrasive wear.

These observations are consistent with the wear-rate results presented in Fig. 7. The reduction in wear-track severity with increasing carbon concentration confirms that carbon enrichment enhances the wear resistance of SCR420 steel. However, the wear behavior is associated not only with hardness but also with the combined effects of carbon concentration and phase constitution within the carburized layer.

### *3.2 Physics-Guided Machine Learning and AI-Guided Optimization*

To validate the complementary physics-based descriptors used in this study, the JMatPro predictions were quantitatively compared with the experimental measurements. As shown in Fig. 9a, the predicted hardness values were closely distributed around the y = x line, indicating that the simulation successfully reproduced the overall hardening behavior of carburized SCR420 steel.

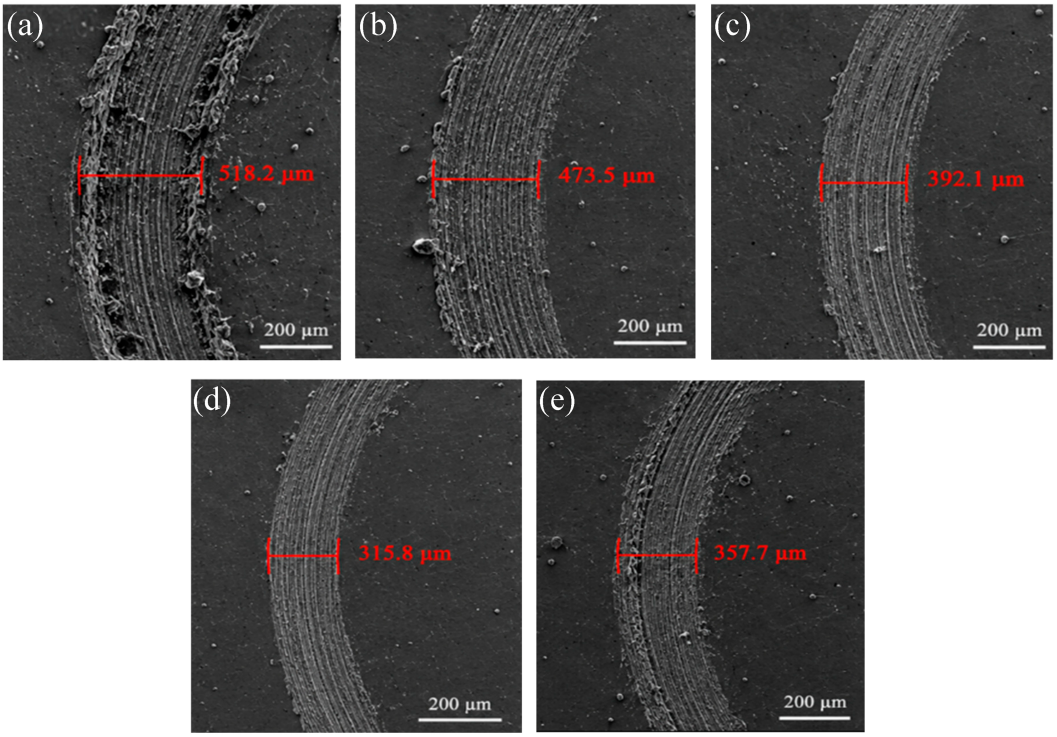



**Figure 8:** SEM observations of wear tracks formed on carburized SCR420 steel with different surface carbon concentrations: (**a**) 0.5 wt.%C; (**b**) 0.6 wt.%C; (**c**) 0.7 wt.%C; (**d**) 0.8 wt.%C; and (**e**) 0.9 wt.%C.

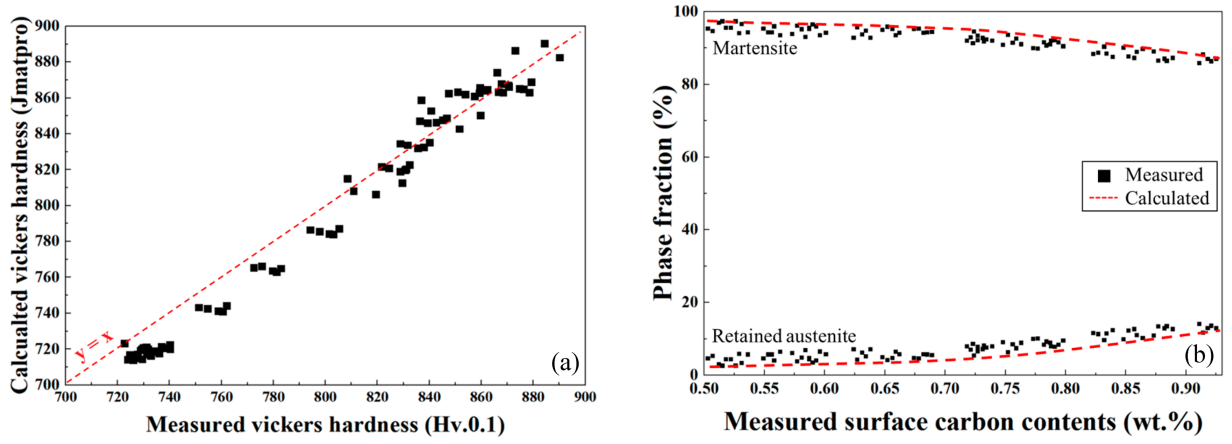



**Figure 9:** Validation of JMatPro predictions for carburized SCR420 steel: (**a**) experimentally measured vs. calculated surface hardness; (**b**) experimentally measured vs. calculated martensite and retained austenite fractions as a function of measured surface carbon concentration.

Fig. 9b compares the measured and calculated martensite and retained austenite fractions as a function of surface carbon concentration. The JMatPro predictions successfully reproduced the overall phase evolution, although the martensite fraction was slightly overestimated and the retained austenite fraction slightly underestimated, which can be attributed to local carbon enrichment and microstructural heterogeneity within the carburized layer. The quantitative validation results are summarized in Table 2. For hardness, the

JMatPro predictions achieved an $R^2$ of 0.954, an MAE of 10.42 Hv, an RMSE of 11.82 Hv, and a mean bias of −6.85 Hv. Similar agreement was obtained for the martensite and retained austenite fractions despite small systematic biases. Overall, these results confirm that JMatPro reliably reproduces the trends in hardness and phase evolution, supporting its use as a complementary physics-based descriptor in the proposed physics-guided machine-learning framework.

**Table 2:** Statistical validation of JMatPro predictions for hardness and phase fractions.

| Model | $R^2$ | MAE | RMSE | Mean Bias |
|---|---|---|---|---|
| Vickers hardness | 0.954 | 10.42 Hv | 11.82 Hv | −6.85 Hv |
| Martensite fraction | 0.948 | 1.62%p | 2.01%p | +1.24%p |
| Retained austenite fraction | 0.923 | 1.28%p | 1.61%p | −0.96%p |

Fig. 10 presents the Pearson correlation matrix and feature-importance analysis for the variables used in the machine-learning framework. As shown in the correlation matrix, wear rate exhibited strong correlations with friction coefficient, hardness, carbon concentration, and phase fractions, indicating that these variables are strongly associated with wear-rate prediction. In particular, wear rate showed a positive correlation with friction coefficient and retained austenite fraction, whereas negative correlations were observed with hardness and martensite fraction.

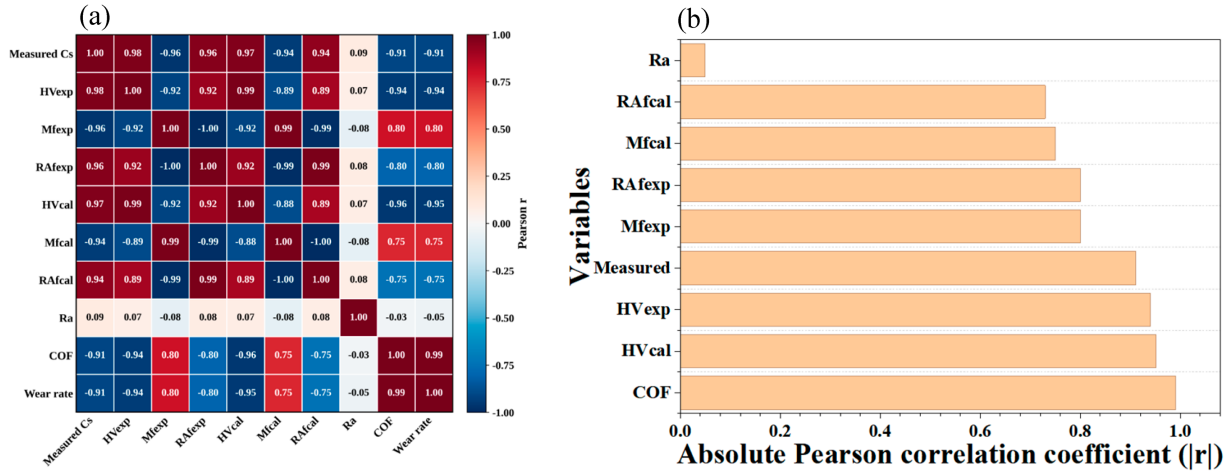



**Figure 10:** Correlation analysis of the experimental and physics-based descriptors used in the proposed machine-learning framework. (**a**) Pearson correlation matrix among surface carbon concentration, hardness, phase-constitution descriptors, surface roughness, friction coefficient, and wear rate. (**b**) Absolute Pearson correlation coefficients (|r|) between each input descriptor and wear rate.

The feature-importance analysis identified the variables that contributed most to the machine-learning model output. Among the investigated parameters, friction coefficient exhibited the highest contribution to wear-rate prediction, followed by hardness-related variables and phase fractions. In contrast, surface roughness showed a relatively low contribution, consistent with the limited variation in roughness observed in Fig. 6. These results indicate that the machine-learning model relies on multiple correlated descriptors rather than a single variable for accurate wear-rate prediction. Because several descriptors, including carbon concentration, hardness, martensite fraction, and retained austenite fraction, are physically coupled through the carburizing and quenching process, partial sharing of feature importance among these correlated

variables is expected. Therefore, the SHAP results were interpreted as complementary information describing the combined evolution of phase constitution and mechanical response rather than as an absolute ranking of independent variables. Accordingly, martensite and retained austenite were interpreted together as phase-constitution descriptors because they provide complementary metallurgical information regarding the carburized microstructure.

Table 3 summarizes the predictive performance of the machine-learning models for wear-rate prediction. All combined models exhibited excellent predictive capability, with $R^2$ values exceeding 0.98 and low RMSE values. Among them, the CatBoost (Combined) model achieved the highest prediction accuracy ($R^2$ = 0.990; RMSE = 1.163 × $10^{-6}$ $mm^3$/N·m). Compared with the CatBoost model using only the experimental descriptors ($R^2$ = 0.965; RMSE = 1.758 × $10^{-6}$ $mm^3$/N·m), the incorporation of the JMatPro-derived hardness and phase-constitution descriptors significantly improved the predictive performance, demonstrating that these physics-based descriptors provide complementary information beyond the experimentally measured variables alone. Furthermore, the CatBoost model without the friction coefficient maintained comparable predictive performance ($R^2$ = 0.989; RMSE = 1.174 × $10^{-6}$ $mm^3$/N·m), indicating that the proposed framework can accurately predict wear rate using descriptors available prior to tribological testing. Therefore, the CatBoost model was selected for subsequent explainable artificial intelligence (XAI) analysis.

**Table 3:** Performance comparison of machine-learning models for wear-rate prediction, including the design-oriented CatBoost model without friction coefficient.

| Model | $R^2$ | RMSE (×$10^{-6}$ $mm^3$/N·m) |
|---|---|---|
| Linear Regression (Combined) | 0.983 | 1.532 |
| Random Forest | 0.989 | 1.224 |
| XGBoost (Combined) | 0.987 | 1.322 |
| CatBoost (Experimental Only) | 0.965 | 1.758 |
| CatBoost (Combined) | 0.990 | 1.163 |
| CatBoost (without COF) | 0.989 | 1.174 |

To further evaluate the robustness of the proposed model, additional grouped cross-validation and leave-one-condition-out (LOCO) validation were performed. As summarized in Table 4, the CatBoost model maintained high predictive performance under both validation strategies, with $R^2$ values of 0.983. Although the prediction accuracy was slightly lower than that obtained using conventional random cross-validation, the performance remained consistently high, indicating that the proposed framework generalizes well to unseen carburizing conditions and that the original model performance was not primarily attributed to repeated measurements.

**Table 4:** Comparison of different validation strategies for the CatBoost model.

| Validation Strategy | $R^2$ | RMSE (×$10^{-6}$ $mm^3$/N·m) |
|---|---|---|
| Random 10-fold CV | 0.990 ± 0.003 | 1.163 ± 0.052 |
| Grouped 10-fold CV | 0.983 ± 0.006 | 1.513 ± 0.081 |
| LOCO validation | 0.983 ± 0.007 | 1.534 ± 0.089 |

The predictive performance of the machine-learning models is illustrated in Fig. 11a. The parity plots show that the predicted wear rates were closely distributed around the y = x line, confirming the reliability

of the proposed framework. Consistent with Table 3, the CatBoost model exhibited the highest agreement between the predicted and measured wear rates. SHAP analysis was then performed using the optimized CatBoost model. As shown in Fig. 11b, the friction coefficient made the greatest contribution to wear-rate prediction, followed by hardness-related variables and phase-constitution descriptors, whereas surface roughness contributed only marginally. Because hardness, carbon concentration, and phase-constitution descriptors are physically coupled through the carburizing and quenching process, the SHAP results should be interpreted collectively as an explanation of model behavior rather than as an absolute ranking of independent variables. Fig. 11c,d shows that increasing carbon concentration and hardness reduced the SHAP value for wear rate, although this reduction became less pronounced above approximately 0.8 wt.%C, indicating an optimal carbon concentration range rather than continuously improving wear resistance. These results demonstrate that the proposed physics-guided machine-learning framework effectively captures the relationships among carbon concentration, phase constitution, hardness, and wear behavior by integrating experimental and JMatPro-derived physics-based descriptors. SHAP analysis further provides a quantitative interpretation of the model output. Based on the trained CatBoost model and SHAP analysis, an optimal surface carbon concentration range was proposed [20].

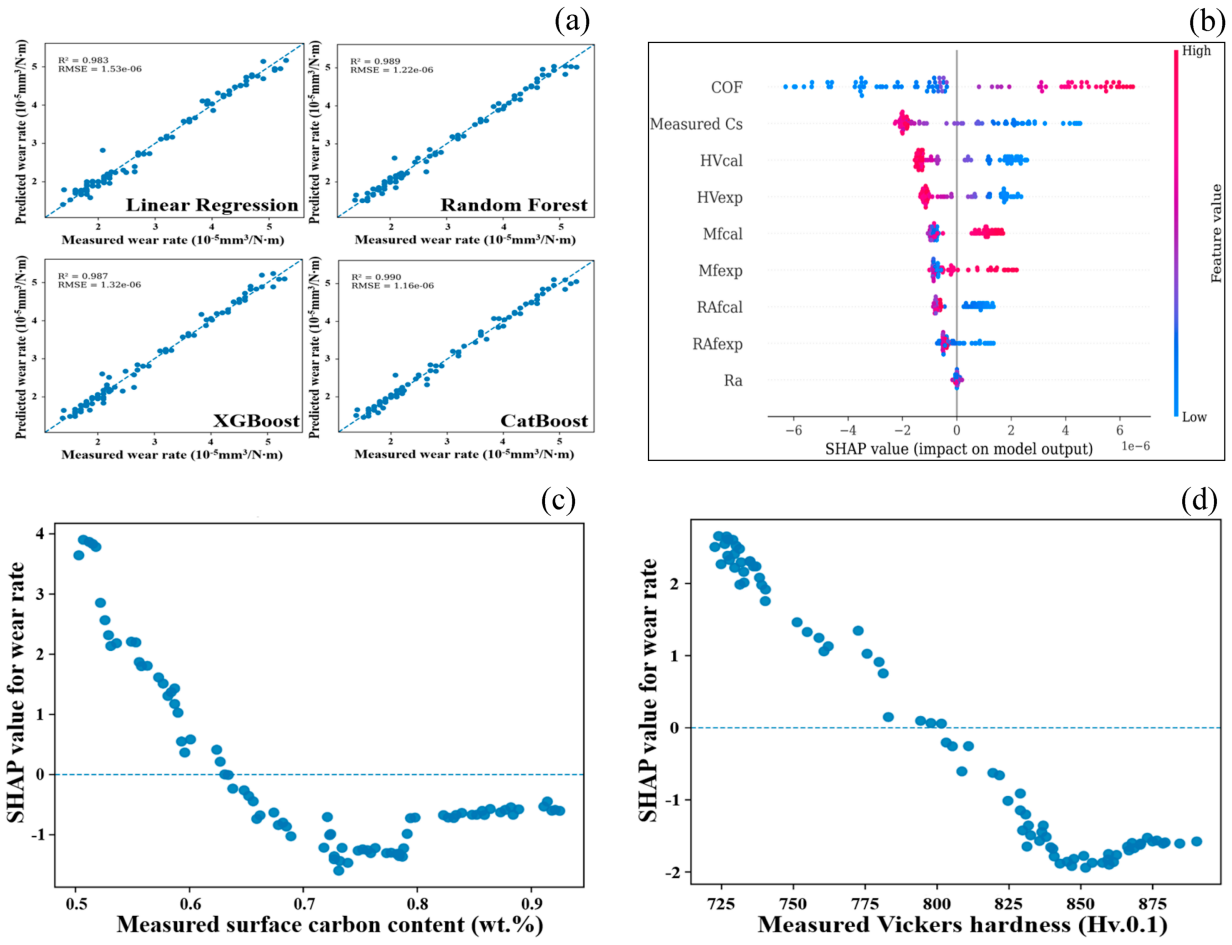



**Figure 11:** Machine-learning performance evaluation and explainable artificial intelligence (XAI) analysis for wear-rate prediction in carburized SCR420 steel: (**a**) parity plots of four machine-learning models; (**b**) SHAP summary plot; (**c**) SHAP dependence plot for measured surface carbon concentration; and (**d**) SHAP dependence plot for experimental hardness.

Fig. 12 presents the AI-guided design window and validation results for optimizing the surface carbon concentration of carburized SCR420 steel. Based on the trained CatBoost model and SHAP analysis, the recommended surface carbon concentration range was proposed as approximately 0.79–0.85 wt.%C, where the predicted wear rate was minimized. As shown in Fig. 12a, the wear-rate prediction map indicates that the lowest wear-rate region occurs within the intermediate-to-high carbon concentration range rather than at the maximum carbon concentration. This result suggests that wear resistance is optimized through a balance among carbon concentration, hardness, and phase constitution rather than by simply increasing carbon concentration.

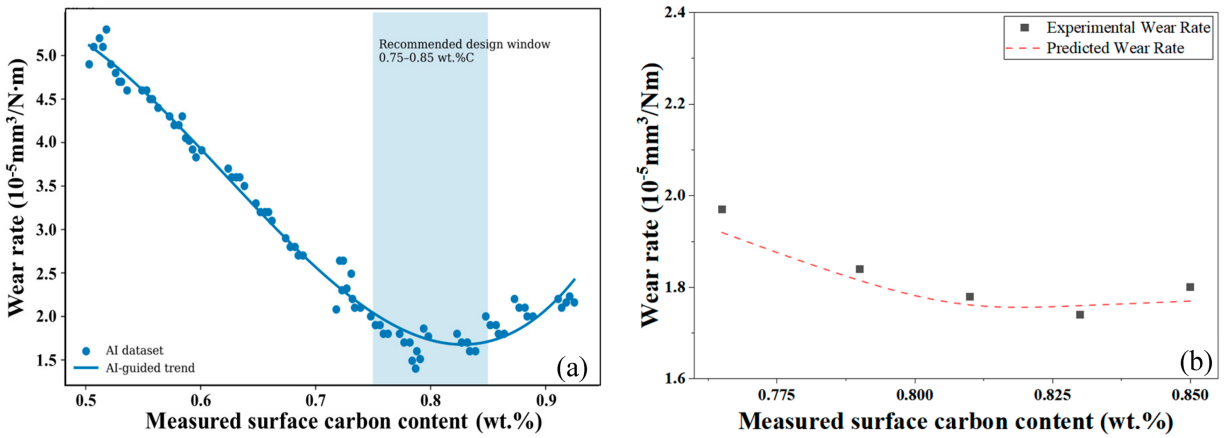



**Figure 12:** AI-guided design window and experimental validation for wear-resistant carburized SCR420 steel: (**a**) identification of the recommended surface carbon concentration range; (**b**) validation of wear-rate prediction within the recommended design window.

Fig. 12b compares the predicted wear rates with experimentally measured values obtained from five independently carburized specimens that were not included in the 85-sample dataset used for machine-learning model development, XAI analysis. Good agreement was observed between the predicted and measured wear rates, demonstrating the validity of the proposed AI-guided design window for previously unseen carburizing conditions. These results further confirm that integrating experimentally measured descriptors with JMatPro-derived physics-based descriptors enables reliable wear-rate prediction and practical optimization of carburizing processes.

## 4 Conclusions

In this study, a physics-guided machine-learning framework was developed to investigate the relationships among carbon concentration, phase constitution, hardness, and wear behavior in carburized SCR420 steel. The main conclusions are summarized as follows:

(1) Increasing the surface carbon concentration increased the hardness and retained austenite fraction of carburized SCR420 steel through changes in carbon distribution and phase constitution.

(2) The friction coefficient and wear rate decreased with increasing carbon concentration. However, wear behavior depended on the combined effects of carbon concentration, hardness, and phase constitution rather than hardness alone.

(3) CatBoost achieved the highest predictive performance ($R^2$ = 0.990). Additional grouped cross-validation and leave-one-condition-out validation also maintained high predictive performance ($R^2$ = 0.983), confirming the robustness of the proposed framework against repeated measurements.

(4) SHAP analysis identified friction coefficient, hardness, and phase-constitution descriptors as the main contributors to the CatBoost model prediction. Considering their physical correlations, the SHAP results were interpreted as an explanation of model behavior. The trained model identified an optimal surface carbon concentration range of 0.79–0.85 wt.%C for enhanced wear resistance.

**Acknowledgement:** This research was supported by the Ministry of SMEs and Startups (MSS, Republic of Korea) through KITECH (Project No. SE-260047 (RS-2025-25443814)).

**Funding Statement:** This research was supported by the Ministry of SMEs and Startups (MSS, Republic of Korea) through KITECH (Project No. SE-260047 (RS-2025-25443814)).

**Author Contributions:** Conceptualization: Gi-Hoon Kwon and Hyosoo Jeon; methodology: Byoungho Choi and Gi-Hoon Kwon; validation: Kyong Jun An and Kyoung Il Moon; formal analysis: Hyosoo Jeon; resources: Kyoung Il Moon; writing—original draft preparation: Gi-Hoon Kwon; writing—review and editing: Kyoung Il Moon and Kyong Jun An; supervision: Kyoung Il Moon. All authors reviewed and approved the final version of the manuscript.

**Availability of Data and Materials:** Data available on request from the authors.

**Ethics Approval:** Not applicable.

**Conflicts of Interest:** The authors declare no conflicts of interest.

## References

1. Lee HY, Lee KH. Effects of carburizing process on sliding wear behavior of carburized SCM420H steel. Tribol Lubr. 2020;36(1):18–26. doi:10.9725/kts.2020.36.1.18.
2. Kimura T, Namiki K. Carburizing and fatigue properties of plasma carburized SCM 420. Denki Seiko. 1990;61(1):32–40. doi:10.4262/denkiseiko.61.32.
3. Ikuta T, Koide T. Case depth and retained austenite of SCM420 steel subjected to repeated carburizing and quenching process. J Jpn Soc Des Eng. 2020;55(1):73–82.
4. Hayama M, Maki Y, Kikuchi S, Komotori J. Change behavior of retained austenite and residual stress on carburized SCM420H steel during fatigue process. ISIJ Int. 2024;64(3):597–604. doi:10.2355/isijinternational.isijint-2023-421.
5. Kanetani K, Mikami T, Ushioda K. Effect of retained austenite on sub-surface initiated spalling during rolling contact fatigue in carburized SAE4320 steel. ISIJ Int. 2020;60(8):1774–83. doi:10.2355/isijinternational.isijint-2019-715.
6. Shen M, Zhu Z, Li S, Yin C, Yang J, Zhang A. Deep learning assisted prediction of retained austenite in the carburized layer for evaluating the wear resistance of mild steel. J Mater Res Technol. 2022;21(10):353–62. doi:10.1016/j.jmrt.2022.09.052.
7. Akatsuka H, Chikugo R, Narazaki M. Preparing hardness prediction data using carburized jominy bar for carburizing quenching. Mater Trans. 2020;61(5):1032–6. doi:10.2320/matertrans.h-m2019861.
8. Skowronek A, Kozłowska A. Phase transitions in medium-Mn alloy: thermodynamic simulation and experimental verification. J Therm Anal Calorim. 2025;150(2):1059–68. doi:10.1007/s10973-024-13824-y.
9. Kim SH, Kim JH, Lee JH, Suh DW, Lee JS. Prediction of retained austenite fraction in quenching-and-partitioning (Q&P) steels using the Gibbs energy balance approach. Met Mater Int. 2022;28(9):2059–67. doi:10.1007/s12540-021-01132-1.
10. Geng X, Wang H, Xue W, Xiang S, Huang H, Meng L, et al. Modeling of CCT diagrams for tool steels using different machine learning techniques. Comput Mater Sci. 2020;171(2):109235. doi:10.1016/j.commatsci.2019.109235.
11. Tiwari S, Dash K, Heo S, Park N, Reddy NGS. Machine learning-driven prediction of microstructural evolution and mechanical properties in heat-treated steels using gradient boosting. Crystals. 2026;16(1):61. doi:10.3390/cryst16010061.

12. Hedström P, Cubero VL, Sigurdsson J, Österberg V, Kolli S, Odqvist J, et al. Physics-informed machine learning for steel development: a computational framework and CCT diagram modeling. Metall Mater Trans A. 2026;57(6):2816–32. doi:10.1007/s11661-026-08181-4.
13. Zhong X, Gallagher B, Liu S, Kailkhura B, Hiszpanski A, Han TY. Explainable machine learning in materials science. npj Comput Mater. 2022;8(1):204. doi:10.1038/s41524-022-00884-7.
14. Oviedo F, Ferres JL, Buonassisi T, Butler KT. Interpretable and explainable machine learning for materials science and chemistry. Acc Mater Res. 2022;3(6):597–607. doi:10.1021/accountsmr.1c00244.
15. Iwasaki Y, Sawada R, Stanev V, Ishida M, Kirihara A, Omori Y, et al. Materials development by interpretable machine learning. arXiv:1903.02175. 2019.
16. Ghosh A. Towards physics-informed explainable machine learning and causal models for materials research. Comput Mater Sci. 2024;233(6):112740. doi:10.1016/j.commatsci.2023.112740.
17. Xiong W, Jiang Y, Sun Y, Shen K, He M, Deng Y, et al. Physics-informed and explainable machine learning framework for performance prediction and design of Ti (C, N)-based cermets. Mater Charact. 2025;229(18):115584. doi:10.1016/j.matchar.2025.115584.
18. Roy S, Sundararajan S. The effect of heat treatment routes on the retained austenite and Tribomechanical properties of carburized AISI, 8620 steel. Surf Coat Technol. 2016;308(1–3):236–43. doi:10.1016/j.surfcoat.2016.06.095.
19. Zhu Z, Liang Y, Yin C, Ren X, Yang M, Zou J. Influence of friction-induced retained austenite transformation to martensite on the wear properties of a carburized layer of 23CrNi$_3$MoA steel. Appl Surf Sci. 2022;595(1):153548. doi:10.1016/j.apsusc.2022.153548.
20. Li Y, Liu B, Zhang Z, Ouyang W, Shi W, Chang Z, et al. Physics-informed machine learning for explainable prediction of friction and wear in carbon-ceramic composites. Ceram Int. 2025;51(28):56400–16. doi:10.1016/j.ceramint.2025.09.355.